Mechanical Systems and Signal Processing 232 (2025) 112708

Contents lists available at ScienceDirect

Mechanical Systems and Signal Processing

journal homepage: www.elsevier.com/locate/ymssp

Separation and quantification of damage-induced and non-damage-induced vibro-acoustic modulation and the problem of contrary modulations

Lennart Dorendorf [a],*, Nikolay Lalkovski [a], Benjamin Boll [b,c], Marcus Rutner [a]

[a] Institute for Metal and Composite Structures, Hamburg University of Technology, 21073 Hamburg, Germany
[b] Institute of Polymers and Composites, Hamburg University of Technology, 21073 Hamburg, Germany
[c] Institute of Surface Science, Helmholtz-Zentrum Hereon, 21502 Geesthacht, Germany

ARTICLE INFO

Communicated by S. Marburg

Keywords:
Vibro-acoustic modulation
Structural health monitoring
Nonlinear acoustics
Damage detection

ABSTRACT

Vibro-acoustic modulation (VAM) has been exploited over the last three decades to assess and monitor the integrity of structures. One major challenge is the separation of damage-induced and non-damage-induced modulation in the measured system response for reliable structural health monitoring (SHM). Most scientific works on VAM imply that the initiation and growth of structural damage is expected to cause modulation that adds up with non-damage-induced modulation increasing the total amount of modulation. This article unfolds why this assumption can be invalid for standard VAM applications: It is explained analytically why two nonlinearities working in opposite directions (one stiffening the structure under loading, one softening it) cause contrary modulations: The two nonlinear contributions can neutralize each other in the system response. Numerical simulations are then presented that investigate separately one damage-induced nonlinearity and two non-damage-induced nonlinearities in the same aluminum plate. The modulation caused by them individually is quantified and the subsequent comparison demonstrates the occurrence of contrary modulations in this representative VAM setup. It has to be concluded that damage-induced modulation does not necessarily increase the total modulation in the system response. This finding has potential to boost VAM-related research regarding its reliability and sensitivity.

1. Introduction

The idea to evaluate vibro-acoustic modulation (VAM) for damage detection evolved in the 1990s [1–5]: Rudenko and Chin [1] described in 1994 the nonlinear-elastic behavior of two rough surfaces in contact. Zaitsev et al. [2] suggested in 1995 to utilize this nonlinear behavior to detect cracks in metal. They proposed to apply an ultrasonic wave and a low frequency vibration simultaneously in order to analyze nonlinear manifestations (such as VAM) in the system response. Donskoy and Sutin [4] reported in 1998 the successful experimental distinguishment of a sound weld in a steel pipe joint from a defective one with VAM method. Since then there has been a large body of literature, thoroughly reviewed in [6], demonstrating the potential of VAM to detect and monitor structural damage in metals [7–10] and in fiber-reinforced plastics [11–18]. However, despite thirty years of research, the method has not found its way into engineering applications outside laboratories, because its reliability remains questionable [9,10,19–23]

---

* Corresponding author.
E-mail address: lennart.dorendorf@tuhh.de (L. Dorendorf).
URL: https://www.tuhh.de/mvb/startseite.html (M. Rutner).

https://doi.org/10.1016/j.ymssp.2025.112708
Received 6 June 2024; Received in revised form 31 March 2025; Accepted 4 April 2025

and because the method can be complex to integrate. A practical application of the method for structural health monitoring is currently not in the picture. However, it is worth noting that even if the issue of practical implementation is left aside for the moment the pursuit of VAM is still a worthwhile endeavor, since it certainly improves the understanding of the underlying physics, and this improved understanding will ultimately bear its fruits. The major challenge jeopardizing the success of the monitoring approach is the following: Any nonlinearity in the system may cause modulation—not only structural damage [10,24]. The separation of damage-induced modulation and non-damage-induced modulation remains a crucial task to enable reliable real-world applications [8–10,19–21,24].

Most VAM studies measure a baseline modulation at a time when the structure is expected to be pristine. This baseline modulation — caused by known and/or unknown non-damage-induced nonlinearities — is taken for reference. During the lifetime of the structure, the modulation is measured and compared to the reference. The initiation and growth of local damage is expected to increase the total modulation in the system response [6,7,9,19,25]. This monitoring approach relies on two assumptions: First, all known and unknown nonlinearities that cause the baseline modulation are expected not to change over time. Second, it is expected that the nonlinear behavior of developing structural damage causes additional modulation that increases the total modulation in the system response significantly. This article unfolds why the second assumption can be invalid for VAM applications: It explains analytically why two nonlinearities working in opposite directions (one stiffening the structure under loading, one softening it) cause contrary modulations: The two nonlinear contributions can neutralize each other in the system response. Afterwards, three realistic nonlinearities in the same aluminum plate are investigated separately with numerical simulations to demonstrate the relevance of contrary modulations in standard VAM setups. Two non-damage-induced nonlinearities and one damage-induced nonlinearity are considered:

(1) variation of the geometric stiffness (non-damage-induced, stiffening the structure under loading)

(2) nonlinear-elastic behavior of aluminum (non-damage-induced, softening the structure under loading)

(3) contact of fatigue crack surfaces (damage-induced, softening the structure under loading)

As explained throughout this article nonlinearity (1) is stiffening the structure under tensile loading while nonlinearities (2) and (3) are softening it. The authors aim to quantify and compare the modulation they cause individually in the system response. The results demonstrate the occurrence of contrary modulations and validate the analytical finding. Only addressing these three nonlinearities is therefore sufficient for the goal of this study. However, note that there are more (and more complicated) nonlinear phenomena in real VAM applications that cause modulation such as energy dissipation-based phenomena (e.g. hysteresis) [8,25,26].

This article is structured as follows: Section 2 presents the basic application procedure of the VAM method and introduces the conventional evaluation approach. Our analytical explanation for the occurrence of contrary modulations is proposed in Section 3. The separation and quantification of the three nonlinearities in the aluminum plate are presented and discussed in Section 4. The conclusions are summarized in Section 5.

2. Evaluating structural integrity with VAM

The application of the VAM method is visualized in Fig. 1. The simultaneous excitation of two waves (X_ω and X_Ω), which differ significantly in terms of their frequency ($\omega \gg \Omega$) and amplitude ($A_\omega \ll A_\Omega$), enable the evaluation of nonlinear manifestations in the system response. On the one hand, the ultrasonic wave X_ω with frequency ω and amplitude A_ω is excited. At the same time, a low frequency (LF) vibration X_Ω with frequency Ω and amplitude A_Ω is introduced to the structure. In case the structure behaves linearly, a pure superposition of X_ω and X_Ω occurs. Hence, the superposed system response would only contain the frequency components ω and Ω (Fig. 1, bottom-left). In case the structure behaves nonlinearly, the ultrasonic wave X_ω is modulated by the LF vibration X_Ω. This modulation manifests itself by the occurrence of sidebands at the frequencies $\omega \pm n \cdot \Omega$ where $n \in \mathbb{N}$ (Fig. 1, bottom-right). The local behavior of structural defects can exhibit nonlinear behavior that causes nonlinear manifestations in the system response [26] such as modulation of the ultrasonic wave X_ω.

The modulation in the system response is (conventionally) quantified by the ratio of sideband amplitudes $A_{\omega\pm\Omega}$ and the amplitude A_ω in frequency domain. The most popular parameter quantifying modulation is arguably the Modulation Index (MI), defined by Donskoy in [26] as

$$MI = 20 \cdot \log_{10}\left(\frac{A_{\omega-\Omega} + A_{\omega+\Omega}}{2A_\omega}\right) \tag{1}$$

Note that in any real VAM application modulation is already measured in a pristine state of the structure. This modulation is caused by known (and potentially unknown) non-damage-induced nonlinearities in the system [9,10,19,23]. The conventional evaluation approach employed in most VAM-related publications assumes that the initiation and growth of structural flaws will cause damage-induced-modulation that increases the total quantified modulation (increasing MI). However, the analytical explanation for the occurrence of contrary modulations in the following section demonstrates why the latter assumption can be invalid in VAM applications.

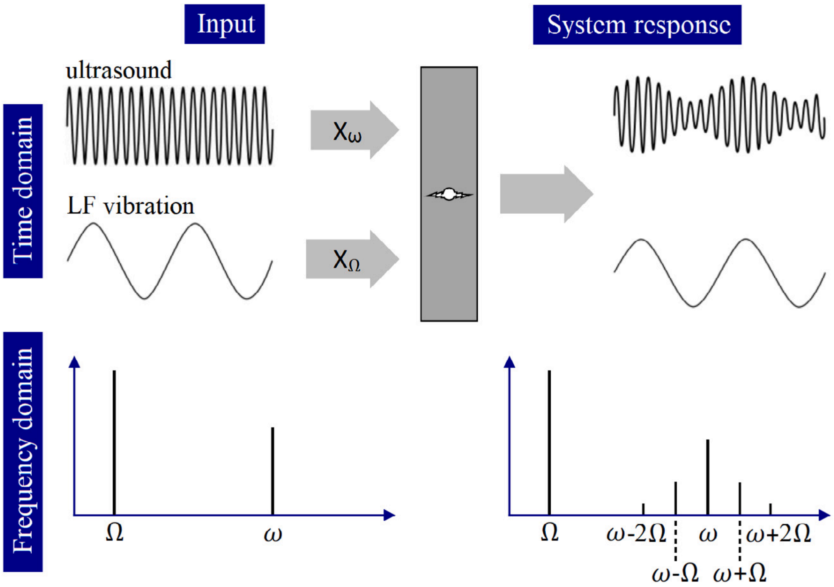

Fig. 1. Vibro-acoustic modulation method schematically: A structure is excited with an ultrasonic wave X_ω and a low frequency vibration X_Ω simultaneously. The modulation of the ultrasonic system response manifests itself by the appearance of sidebands in the corresponding FFT spectrum at frequencies $\omega \pm n \cdot \Omega$ where $n \in \mathbb{N}$.

3. Analytical explanation for contrary modulations

In a previous publication in 2022 [24] the authors suggested a physical explanation revealing why any elastic nonlinearity may cause VAM in a dynamic system that is excited by two waves simultaneously (X_ω and X_Ω) in case the corresponding frequencies differ significantly ($\omega \gg \Omega$): Only the LF vibration X_Ω activates the nonlinearity considerably ($A_\omega \ll A_\Omega$) and varies quasi-statically the system's natural frequency ω_0 corresponding to the dominant mode shape. The amplitude of the ultrasonic system response depends on the natural frequency ω_0 and is therefore modulated with low frequency Ω. This explanation is built upon the assumption that the system reaches a steady-state vibration (constant amplitude over time) due to the ultrasonic excitation X_ω before the LF vibration X_Ω can change the dynamic properties of the system significantly. In this case one can evaluate the steady-state responses (caused by the ultrasonic excitation X_ω) for linear systems in discrete intervals, while only producing a negligible error [27]. The underlying assumption was proven to be valid numerically and experimentally for the aluminum plates investigated in [24] and excitation frequencies $\Omega = 10$ Hz$\cdot 2\pi$ and 180 kHz$\cdot 2\pi < \omega <$ 230 kHz$\cdot 2\pi$. One consequence of this explanation is that the choice of the ultrasonic frequency ω and the modal density surrounding it directly affect the amount of modulation in the system response [24]. Note that the content in the following builds directly upon the physical explanation presented in [24].

A damped single-degree-of-freedom (SDOF) system as shown in Fig. 2a is considered. It is described by its mass m, its damping coefficient d and its stiffness $k(x)$. The displacement x is the degree of freedom. First, the system is considered to behave linearly: The stiffness $k(x)$ is constant. Consequently, the relationship between force F and the displacement x is linear as plotted with a blue solid line in Fig. 2b. The natural frequency ω_D of this damped (linear) SDOF system is

$$\omega_D = \omega_0 \sqrt{1-\xi^2} \tag{2}$$

with the natural frequency of the corresponding undamped system ω_0

$$\omega_0 = \sqrt{\frac{k}{m}} \tag{3}$$

and damping ratio ξ

$$\xi = \frac{d}{2m\omega_0} \tag{4}$$

When the linear system is excited with the ultrasonic wave X_ω, the system responds (eventually) with a steady-state vibration (constant amplitude over time). The analytical solution for the dynamic magnification factor D (proportional to the amplitude of that steady-state vibration) is known [28]

$$D = \frac{1}{\sqrt{(1-\beta^2)^2 + (2\xi\beta)^2}} \tag{5}$$

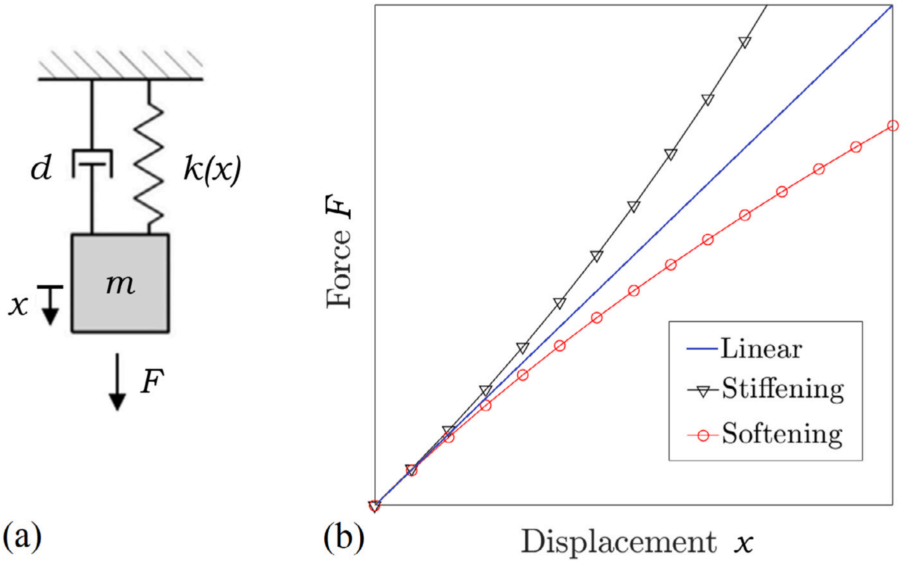

Fig. 2. (a) Damped SDOF system: mass m, damping coefficient d, stiffness $k(x)$, displacement x, force F (b) Three different relationships between the force F and the displacement x: Linear-elastic (blue solid line), schematic nonlinear-elastic "stiffening" (black solid line with triangles), schematic nonlinear-elastic "softening" (red solid line with circles). (For interpretation of the references to color in this figure legend, the reader is referred to the web version of this article.)

with β, defined as the ratio of excitation frequency ω and the natural frequency of the undamped system ω_0

$$\beta = \frac{\omega}{\omega_0} \tag{6}$$

The magnification factor D is plotted over the frequency ratio $\beta = \omega/\omega_0$ and the damping ratio ξ in Fig. 3a.

Now, this linear system is excited by two waves (X_ω and X_Ω) simultaneously with frequencies that differ significantly ($\omega \gg \Omega$). The quasi-static excitation of the LF vibration X_Ω is plotted in Fig. 3b over time for two of its periods ($2 \cdot T_\Omega$). It is a harmonic force that varies between zero and $F_{\max}$. The system response will be a pure superposition of two vibrations corresponding to the excitation frequencies Ω and ω. The (highpass-filtered) ultrasonic system response will be a steady-state vibration with constant amplitude (here $D = 3$) as plotted in Fig. 3c over time. Taking into account the physical explanation in [24] no modulation occurs here, because the stiffness $k(x)$ (and therefore the ratio β) cannot be affected by the quasi-static application of the LF vibration X_Ω.

Second, it is considered that the SDOF system is nonlinear and stiffens with loading: Such behavior is displayed in Fig. 2b with the black solid line (triangles). The system is nonlinear, because the stiffness $k(x)$ depends on the displacement x. When the force F (quasi-statically) rises, the stiffness $k(x)$ increases. Consequently, the natural frequency ω_0 increases as well and the ratio β drops. When excited with X_ω and X_Ω simultaneously, the (highpass-filtered) system response is modulated as plotted in Fig. 3d. Note that for $F = 0$ (origin of the graph in Fig. 2b), the gradient (stiffness k) is identical in the nonlinear and the linear system. Therefore, also the ratios β and the amplitudes match ($D = 3$). The quasi-static variation of $\beta(\Omega)$ and $D(\Omega)$ in the nonlinear "stiffening" system are indicated with the black double arrow in Fig. 3a.

In a third step the system is considered to soften with loading, as shown in Fig. 2b with the red solid line (circles). For $F = 0$ the stiffness is equal to the stiffness in the previous two systems. However, with force F increasing, the stiffness $k(x)$ drops, the natural frequency ω_0 decreases and the ratio β increases. As a result, the modulation in the system response works in the opposite direction compared to the previous "stiffening" system. The system response is plotted over time in Fig. 3d. Analogously, the variation of $\beta(\Omega)$ and $D(\Omega)$ in the nonlinear "softening" system are indicated with the red double arrow in Fig. 3a. The variation of β (displayed in Fig. 3a) is shown to stay above the value β=1.0 here. For a variation of β below the value $\beta = 1.0$ all arguments work analogously. If the variation of β crosses the value $\beta = 1.0$ the explanation works the same way but the respective envelope functions look more complex as explained and demonstrated in the previous publication [24].

The previous content explains why a SDOF system that softens under loading and a SDOF system that stiffens under loading show modulations in opposite directions when excited with X_ω and X_Ω simultaneously. Any real structure has an infinite number of degrees of freedom and therefore an infinite number of natural frequencies with corresponding mode shapes. The system response will be dominated by the natural frequencies (and corresponding mode shapes) that lie closest to the excitation frequency ω [28]. As explained in our previous publication [24] the explanation for the SDOF system is applicable to each natural frequency and corresponding mode of the MDOF system allowing modal superposition.

When considering that two nonlinearities working in opposite directions (one stiffening the structure under loading, one softening it) are combined in the same structure and are both activated by the LF excitation X_Ω, their respective effects on the natural frequencies will work in opposite direction. Taking into account the previous explanations this leads to the conclusion that the two

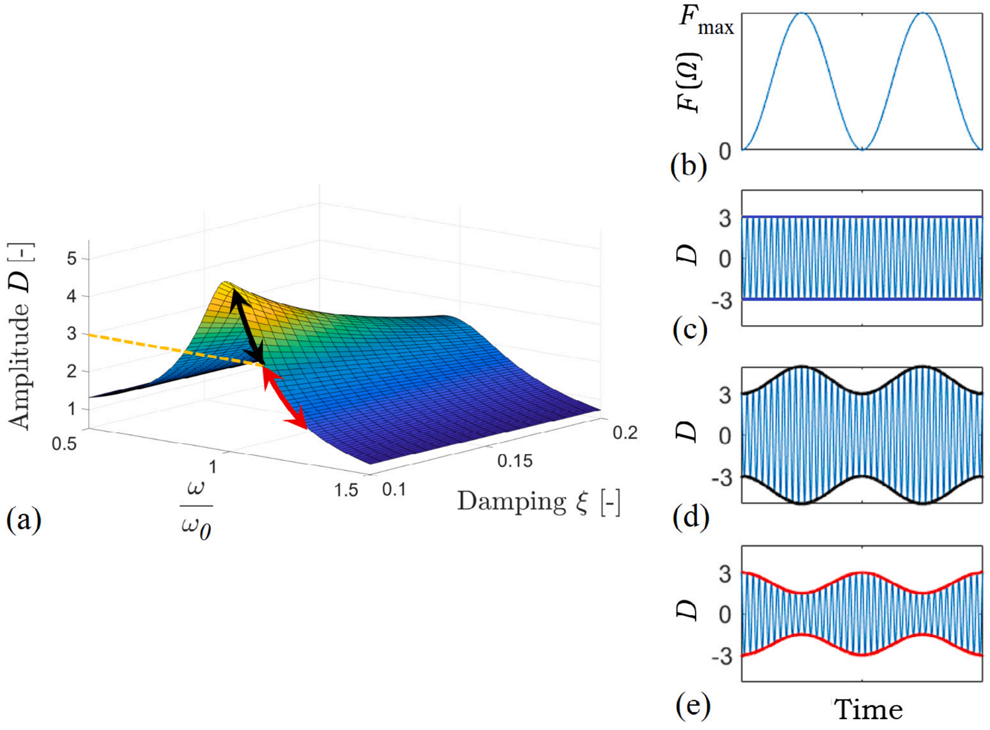

Fig. 3. (a) Dynamic magnification factor D (proportional to the amplitude of the steady-state response) over ratio $\beta = \omega/\omega_0$ and damping ratio ξ; The black arrows indicate the variation of β and D corresponding to VAM in the nonlinear "stiffening" system; The red arrows indicate the variation of β and D corresponding to VAM in the nonlinear "softening" system (b) Schematic LF excitation X_Ω over time (c) Schematic highpass-filtered system response over time, corresponding to the linear system (d) Schematic highpass-filtered system response over time corresponding to VAM in the nonlinear "stiffening" system (e) Schematic highpass-filtered system response over time corresponding to VAM in the nonlinear "softening" system. (For interpretation of the references to color in this figure legend, the reader is referred to the web version of this article.)

nonlinear contributions can neutralize each other in the system response. It can be concluded, that the presence of two nonlinearities in the system does not necessarily cause more modulation in the system response than both nonlinearities would individually.

4. Separation and quantification of nonlinearities

In this section three nonlinearities that are present in the same aluminum plate are investigated separately. The goal is to quantify and compare the modulation they cause individually in the system response. Two non-damage-induced nonlinearities and one damage-induced nonlinearity are considered here: (1) The variation of the geometric stiffness, (2) the nonlinear-elastic behavior of aluminum and (3) the contact of fatigue crack surfaces.

It is very difficult — if not impossible — to separate the three nonlinearities above and the modulation they cause in an experimental setup. Therefore, the nonlinear contributions to the system response are investigated numerically with explicit dynamic simulations in Abaqus CAE. The great advantage of a FE analysis is that the user controls all input data and can hereby artificially suppress features that are present in reality.

While nonlinearity (1) stiffens the system under tensile loading nonlinearities (2) and (3) soften it. Our physical explanation in Section 3 suggests that stiffening and softening nonlinearities cause contrary modulations when present in the same system. Four different simulations are run to demonstrate this: The first simulation only governs nonlinearity (1). The second simulation combines nonlinearities (1) and (2) in the system, while the third simulation combines nonlinearities (1) and (3) in the system. The results of these first three simulations demonstrate when compared that the stiffening nonlinearities (2) and (3) cause modulation that works in the opposite direction than the modulation caused by softening nonlinearity (1). The envelope functions in time-domain are reversed as expected. In a fourth simulation all three nonlinearities are combined in the system.

4.1. Aluminum plate and numerical modeling

Aluminum plates with dimensions 160 mm/20 mm/3 mm and a circular notch (diameter 4.5 mm) in the center are investigated numerically with Abaqus CAE in the scope of this article. The geometry and setup comply with the work in the authors' previous publication [24]. The FE model with mesh size 0.75mm is shown in Fig. 4. The cross-section at the left end is fixed (all displacements

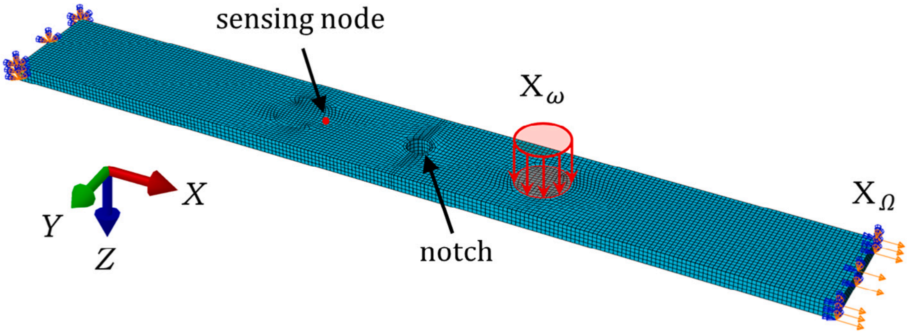

Fig. 4. FE model of the aluminum plate with dimensions 160mm/20mm/3mm. LF excitation X_Ω, ultrasonic excitation X_ω, the system response is measured at the sensing node.

and rotations are zero). The cross-section at the right end features a prescribed displacement in X-direction, which is to be further explained below. The remaining degrees of freedom at the right end are all set to zero.

To apply the ultrasonic excitation X_ω in the FE model, a pressure is acting on the circular surface (diameter 10mm) of the specimen. This pressure acts normal to the surface. This modeling approach approximately represents the effect of a piezoceramic disc which is typically employed to excite X_ω in experimental VAM setups.

As a system response, the out-of-plane acceleration in Z-direction [m/s^2] at a specific node on the specimen's surface is evaluated. This node is highlighted in Fig. 4 and referred to as the "sensing node" from hereon. The LF vibration X_Ω is excited as a prescribed periodic displacement in X-direction applied to the cross-section at the right end of the structure in Fig. 4. It is a purely tensile activation that varies harmonically between zero and A_Ω. Compressive loading would be less practical due to buckling. The amplitude is set to the realistic value of $A_\Omega = 0.2$ mm. The elongation of $\Delta l = 0.2$ mm causes a strain of $\epsilon_X = 0.00125$. This strain (1.25‰) lies in the elastic range of aluminum. The excitation frequencies are $\omega = 199$ kHz$\cdot 2\pi$ and $\Omega = 10$ Hz$\cdot 2\pi$. Note that $\Omega = 10$ Hz $\cdot\, 2\pi$ lies far below the lowest axial natural frequency of our specimen. The consequence is that there are no inertia forces within the specimen as this force is applied, meaning that the response is quasi-static.

4.2. Variation of the geometric stiffness

The application of a tensile force on a structure generates "geometric bending stiffness" that comes in addition to the elastic bending stiffness EI of the structure (where E is the Young's modulus and I the second moment of inertia) [28]. When considering the aluminum plate in Fig. 4 the presence of tensile stress in X-direction σ_X will activate restoring forces in Z-direction as soon as bending is applied. The excitation of the LF wave X_Ω changes the present tensile stress σ_X in the aluminum plate periodically with $\Omega = 10$ Hz$\cdot 2\pi$. Consequently, due to the geometric stiffness component, the total bending stiffness of the structure is varied accordingly. Considering the physical explanation in [24] this necessarily causes VAM. Musicians utilize geometric stiffness to tune instruments such as guitars. Note that nonlinearity (1) is "stiffening" the structure under tensile loading.

The material in the FE model is set to behave linearly-elastic with Young's modulus $E = 73000$ N/mm^2 and Poisson's ratio $\nu = 0.296$. The material density is defined with $\rho = 2752$ kg/m^3. The damping ratio is set to $\xi = 0.01$ for the frequency range of interest with Rayleigh damping coefficients $\alpha_R = 80$ and $\beta_R = 1.38 \cdot 10^{-8}$. Fig. 5 shows the results from the simulation in which the only present nonlinearity is the variation of geometric stiffness. In Fig. 5a, the stress σ_X for an element in the sensing node's direct vicinity is plotted over 0.3s. It represents the LF excitation X_Ω. Also the ultrasonic excitation X_ω varies the stress σ_X at this element with frequency $\omega = 199$ kHz$\cdot 2\pi$. The amplitude of this stress variation is only $\Delta\sigma_X = 0.1$ kN/cm^2 though and therefore not visible in this plot. Note that the excitation amplitudes differ significantly ($A_\omega \ll A_\Omega$). The coordinate system and the FE model are visualized in Fig. 5b. Note that the shown deformation of the specimen in this image is magnified by the factor $2.5 \cdot 10^7$ to make the ultrasonic vibration visible here. In Fig. 5c the acceleration in Z-direction at the sensing node is plotted over 0.3 s. This acceleration is considered as the system response for latter comparisons. Fig. 5d shows the FFT spectrum of the system response in dB. The MI is the most common parameter to quantify the modulation in the literature. It reaches a value of $MI = -22.2$ dB here.

4.3. Nonlinear-elastic behavior of aluminum

Within the elastic range of their behavior metals show a nearly linear stress–strain dependency under tension. A linear approximation is sufficiently accurate for most engineering tasks and is the basis for using Hooke's law and the Young's modulus E [29]. When taking a closer look at tensile test data for aluminum however, one realizes that the material does not behave perfectly linear in its elastic range. Five tensile tests are performed with aluminum alloy EN-AW6060 specimens according to German design code DIN 50125:2016-12 [30]. The specimens' dog-bone geometry is shown in Fig. 6a with dimensions in mm. It is a flat dog-bone specimen with thickness $t = 8$ mm (Fig. 6b). Fig. 6c shows a representative stress–strain curve from one of the five tensile tests.

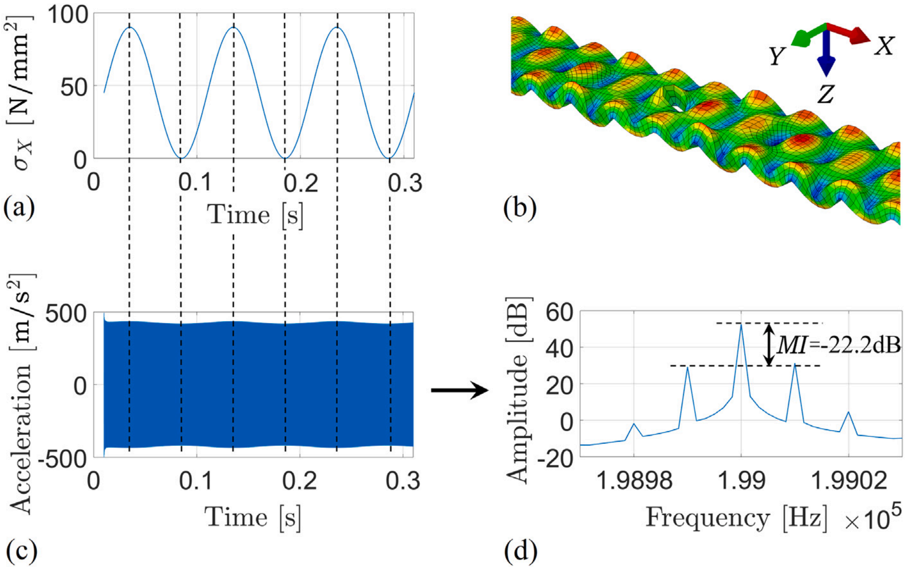

Fig. 5. Results from the simulation with only one nonlinearity present: The variation of geometric stiffness (a) Stress σ_X over 0.3 s at an element in the sensing node's direct vicinity (b) Coordinate system for orientation; deformation of the specimen is magnified by factor $2.5 \cdot 10^7$ (c) Acceleration in Z-direction at the sensing node over time (system response) (d) FFT spectrum corresponding to the system response.

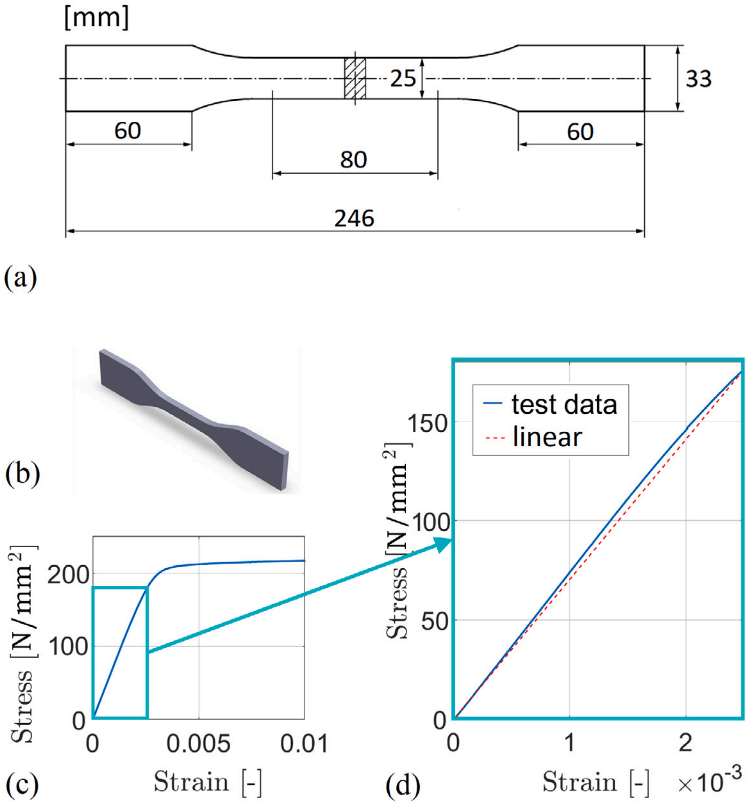

Fig. 6. (a) In-plane geometry in mm (b) Flat dog-bone specimen with thickness t = 8 mm (c) Tensile stress–strain curve for aluminum alloy EN-AW6060 (AlMgSi0,5/3.3206) (d) Close-up of the tensile stress–strain curve (blue solid curve) with linear reference for comparison (red dashed line). (For interpretation of the references to color in this figure legend, the reader is referred to the web version of this article.)

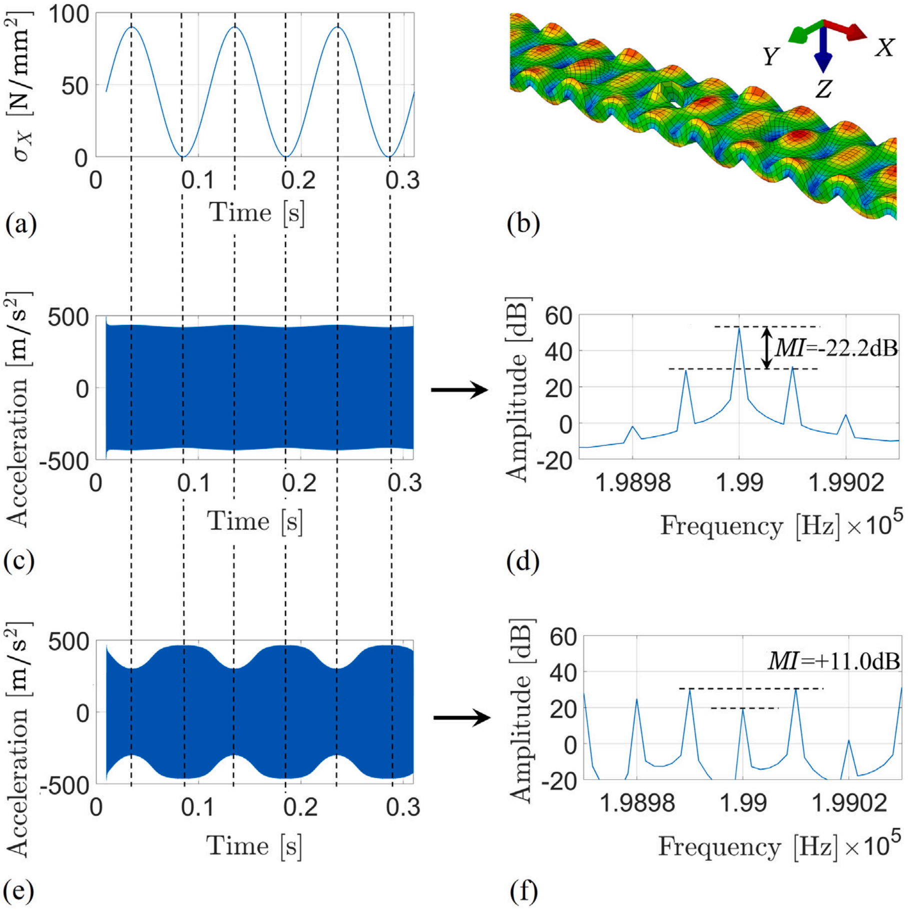

Fig. 7. (a) Stress σ_X over time in direct vicinity of the sensing node (b) Coordinate system for orientation; deformation of the specimen is magnified by factor $2.5 \cdot 10^7$ (c) System response (acceleration in Z-direction) at the sensing node (the only present nonlinearity in this simulation is the variation of geometric stiffness) (d) corresponding FFT spectrum in dB (e) System response (acceleration in Z-direction) at the sensing node (the present nonlinearities in this simulation are the variation of geometric stiffness and the nonlinear-elastic material behavior of aluminum) (f) Corresponding FFT spectrum in dB.

The stress–strain curve shows yielding at roughly $\epsilon = 0.003$ initializing plastic material behavior. In the elastic range of the material ($\epsilon < 3‰$) the relationship appears to be linear to the bare eye. A close-up of the test data for $0 < \epsilon < 0.0025$ is presented in Fig. 6d. Comparison of the test data (blue solid curve) with a linear reference (red dashed line) demonstrates the very weak — but present — nonlinearity of the elastic stress–strain dependency. Note that nonlinearity (2) is “softening” the structure with tensile loading and is therefore expected to cause modulation that works in opposite direction compared to the modulation caused by nonlinearity (1).

The test data in the range of $0 < \epsilon < 0.0025$ is used as input data to define a nonlinear-elastic material in Abaqus CAE. After a polynomial fit of the test data in MATLAB the hyperelastic material model “Marlow” is used which follows the fitted uniaxial tensile test data exactly [31]. In the following step, a dynamic explicit simulation is run that is identical to the previous one with the only difference that all material in the model is defined with the weakly nonlinear-elastic data instead of the linear-elastic material. Note that the variation of geometric stiffness is not artificially suppressed in this second simulation and that therefore both nonlinearities — (1) the variation of geometric stiffness and (2) the nonlinear-elastic behavior of aluminum — are present here. The results of the two simulations are compared in Fig. 7. The stress state in closest vicinity of the sensing node is plotted in Fig. 7a and represents the LF excitation X_Ω. Fig. 7b shows the global coordinate system in the FE model for orientation. In Fig. 7c the results from the first simulation only including (1) the variation of geometric stiffness are presented with the corresponding FFT spectrum in dB in Fig. 7d. The results from the second simulation are shown analogously in Fig. 7e (system response in time domain) and Fig. 7f (FFT spectrum). The comparison in time domain demonstrates that the nonlinear-elastic behavior of aluminum affects the system response significantly. Stronger modulation can be observed by eye. The corresponding FFT spectrum shows that the first pair of sidebands at $\omega \pm \Omega = (199 \pm 0.01)\mathrm{kHz}\cdot 2\pi$ has risen above the amplitude A_ω. Conventional quantification of the spectrum leads to $MI = +11.0$ dB. It is significantly higher than in the previous simulation with an increase of $\Delta MI = 33.2$ dB. The broader spectrum (not plotted here) shows up to one hundred pairs of sidebands at $\omega \pm n \cdot \Omega$ where $n \in \mathbb{N}$ for the second simulation.

The time domain comparison (Figs. 7c vs. 7e) reveals something that the corresponding spectra (and MI) do not display: The modulation is not simply increased in the second simulation, the envelope function of the modulated system response is also reversed, as expected: The maximum of the envelope in Fig. 7c coincides with the minimum of the envelope in Fig. 7e. This result demonstrates the occurrence of contrary modulations as explained analytically in Section 3: Different nonlinearities combined in the same system can cause contrary modulations. According to the suggested analytical explanation this phenomenon must necessarily exist: While nonlinearity (1) stiffens the system under tensile loading, nonlinearity (2) softens it. Consequently, the (dominating) natural frequency $\omega_0(\Omega)$ is varied in opposite directions. Hence, the steady-state amplitude is affected contrarily.

When exploiting VAM for structural health monitoring it is expected that local damage can cause significant modulation in the global system response due to its nonlinear behavior. Note that — as weak as it may be — the material nonlinearity investigated in this section is distributed over the entire volume of the plate.

4.4. Contact of fatigue crack surfaces

It is intuitive why the variation of geometric stiffness and the nonlinear-elastic behavior of aluminum exhibit nonlinear-elastic behavior in a tensile fatigue loading scenario of the specimen. It is less intuitive why two rough crack surfaces which are opened and closed repetitively should exhibit nonlinear-elastic behavior under purely tensile fatigue loading. However, the literature shows that the latter is the common understanding in the scientific community. The most popular explanations in the literature are the nonlinear-elastic behavior due to Hertzian contact and energy dissipation-based phenomena [26,32]. In this section the authors present a simple approach to quantify the nonlinear-elastic behavior due to Hertzian contact of crack surfaces that occurred experimentally in the aluminum plates. Note that crack formation is a complex phenomenon with different stress regions, plastic deformations and slip surfaces that are not taken into account here.

The question that has not been clearly addressed in the literature to the authors' best knowledge is the following: The argument of Hertzian contact assumes pressure between the surfaces. Many VAM studies however report experimental work with purely tensile fatigue loading setups without clarifying why nonlinear-elastic behavior of the crack is expected. We aim to answer this question before demonstrating an approach to quantify the modulation caused by the local contact of fatigue crack surfaces. To begin with, the rough surface of a local fatigue crack in aluminum[1] is looked upon closely with a microscope to measure its geometry. Fig. 8a shows the aluminum specimen with a close-up of the fatigue crack that has initiated from the notch. After total fatigue failure of the specimen the crack surfaces are accessible for the microscope. A magnified image (factor 1500) is presented in Fig. 8b: The fatigue crack propagated from the right (notch) to the left in this image. A depth measurement (here in X-direction) is carried out with the microscope for a 2mm/1.5mm Y-Z-plane providing a point cloud, which describes the three-dimensional geometry of the crack surface. A three-dimensional plot of the data is given in Fig. 8c. The point cloud data above the red dashed 1mm^2 projection square in Fig. 8c is now utilized to define the nodes and elements of a FE mesh. The FE mesh describes a 1mm^3 cube separated by the exact crack surface geometry that was measured experimentally. The FE mesh (node and element geometry) is exported to Abaqus CAE for further use (Fig. 9).

The crack surface of the lower cube part and the crack surface of the upper cube part are defined by the same point cloud data ensuring that they fit ideally into each other. Consequently, the parts can be in full contact (at each node) without any stress present.

The following considerations are made by the authors to explain why such crack surfaces may exhibit nonlinear-elastic behavior even when the external fatigue loading is tensile only: Tensile stress must be present across the potential crack surfaces (here in X-direction) to cause cracking in the first place. After cracking, when the newly formed crack surfaces move apart for the first time, the geometry of the two surfaces are expected to be identical, as modeled in Fig. 9. These two crack surfaces will not be able to transfer any tensile stress and will behave linearly-elastic under pressure in X-direction. Consequently, a bilinear-elastic behavior can be expected which — considering the explanation presented in [24] — does not lead to any modulation when fatigue loading is tensile only. However, in the authors' opinion two phenomena can be expected after the formation of a crack that deviate from the ideal fit in reality:

1. A lateral relative shift of the crack surfaces (in Y-Z-plane)
2. Irreversible (and not identical) deformation of the crack surface geometry due to plastic deformation (lateral and/or longitudinal)

This opinion is in line with most research articles on VAM indicating that the fatigue crack surfaces in metals are expected to be messy and chaotic [26].

In case the surfaces do not find their way back into the original position, the release of the external tensile force back to zero will activate local contact pressure at any location where the two surfaces deviate from a perfect fit. When the external force rises again, this local contact pressure will be reduced until the surfaces lose contact. It is this reduction of local contact pressure (under external tension) that can explain nonlinear-elastic behavior. To demonstrate this, the upper cube part from Fig. 9 is shifted in Y- and Z-direction by 1/100 of the cube length ($\Delta Y = \Delta Z = 1$ mm/100 = 10 μm). The lateral offset is indicated in Fig. 10. It is too small to recognize it here. Now — with this lateral offset in place — a simulation is run where these two linear-elastic cube parts (E = 73000 N/mm^2) are pressed against each other vertically (in X-direction). To do so, all nodes at the bottom Y-Z-plane of the lower part are fixed in X-direction (boundary condition $u_X = 0$). The nodes at the top Y-Z-plane of the upper part behave as a

---

[1] The material and geometry of this specimen is identical to the ones in [24] and complies with the numerically investigated plate in this article. Fatigue loading was applied with $r = 0$ (tensile stress only). Total failure occurred after 52000 load cycles.

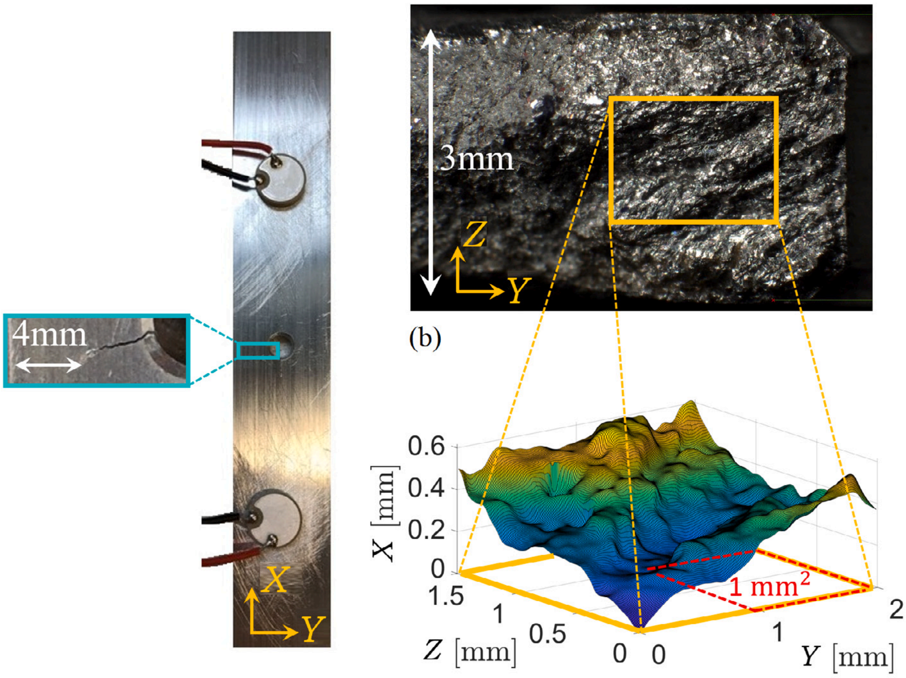

(a) (c)

Fig. 8. (a) Aluminum specimen with a fatigue crack initiating from the notch (b) Microscope image of the crack surface magnified with factor 1500 (c) Point cloud describing the measured three-dimensional geometry of the crack surface.

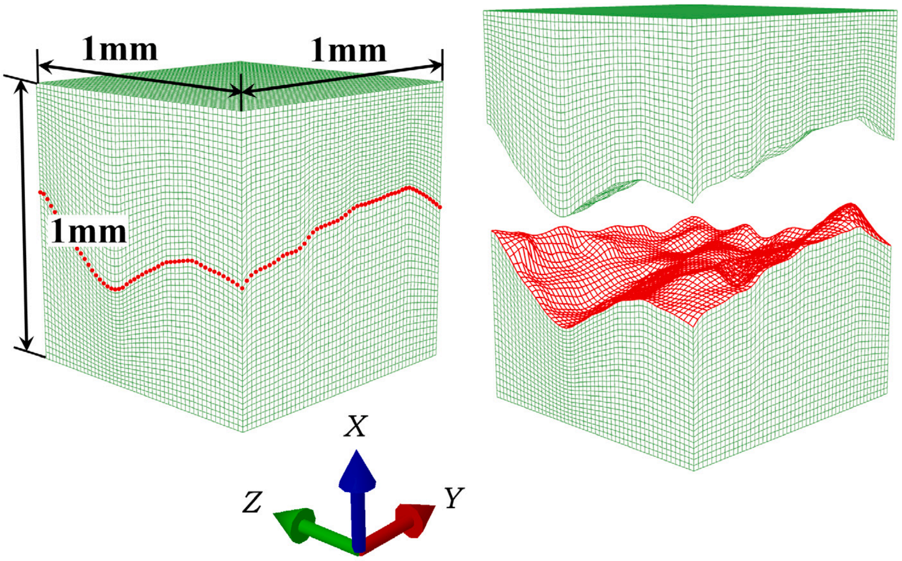

(a) (b)

Fig. 9. FE Model of a 1mm^3 that is separated by the point cloud data (red) that represents the experimental crack surface geometry (a) Both cube parts in contact (perfect fit) (b) Both cube parts apart (in X-direction). (For interpretation of the references to color in this figure legend, the reader is referred to the web version of this article.)

rigid plate. This rigid plate is subjected to a prescribed downward displacement moving in negative X-direction (Fig. 10). During the simulation the reaction force in X-direction is measured. The results — vertical displacement of the rigid plate vs. the reaction force — are converted to stress vs. strain. The latter dependency is plotted in Fig. 11 (blue solid line). It can be observed that the system behaves indeed nonlinearly-elastic: In (nearly) full contact (strains $\epsilon < -0.04$) the stress–strain dependency approaches a linear

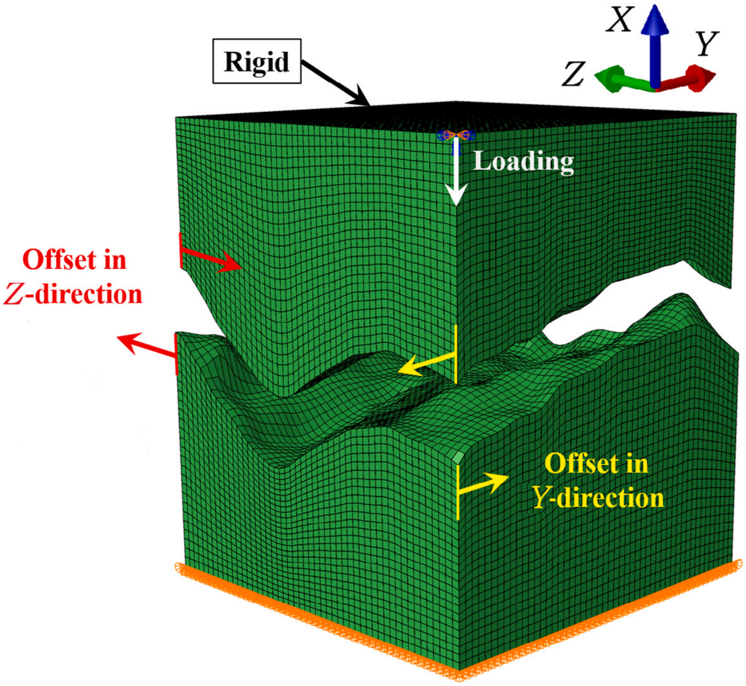

Fig. 10. FE model of the separated cube with a lateral offset in Y- and Z-direction with $\Delta Y = \Delta Z = 1$ mm/100 = 10 μm; The top Y-Z-plane of the cube behaves as a rigid plate.

function with a gradient corresponding to the Young's modulus that was set to the value $E = 73000$ N/mm^2 for the linear-elastic material. Once the crack surfaces lose contact entirely (strains $\epsilon > 0$) the stress–strain relationship becomes zero (constant). Between these two states ($-0.04 < \epsilon < 0$) the system behaves nonlinearly-elastic due to the variation of the contact surface transferring the load. Regarding this result, note three things: The position for $\epsilon = 0$ on the horizontal axis was chosen by the author to coincide with the initial contact of the two crack surfaces during post-processing. Second, the results in Fig. 11 show that the nonlinear behavior spans over a strain range of roughly $\Delta\epsilon = 0.04$. Within this strain range $\Delta\epsilon$ the gradient varies between the set Young's modulus E and zero ($E = 73000$ N/mm$^2 > gradient > 0$ N/mm^2). For this simulation the lateral offset was set to be 1/100 of the cube length. Decreasing this offset will lead to results in which the strain span $\Delta\epsilon$ governing the nonlinear-elastic behavior will decrease, too. Such scaling of the nonlinear-elastic behavior is taken advantage of later in this section. Third, the results were developed for a 1mm^3 cube. In the authors' opinion the volume (and hereby the crack) can be extended in Y- and Z-direction without losing the validity of the stress–strain results in X-direction in Fig. 11. At this point, it is understood why crack surfaces behave nonlinearly-elastic despite (external) tensile fatigue loading of the specimen. Further, the nonlinear-elastic behavior for an experimental crack geometry was demonstrated and quantified. In the following it is the goal to include the nonlinear-elastic behavior of the crack into the FE model of the aluminum specimen from Sections 4.2 and 4.3 to investigate its effect on the system response (modulation). To do so, two volumes (width 1 mm in X-direction) are implemented in the FE model on both sides of the notch (Fig. 12a). Each of these volumes represent a volume that is separated by a fatigue crack. A total crack length of 6mm is considered here (3mm on each side of the notch). However, the crack itself is not modeled. Instead, the highlighted volumes are set to be nonlinear-elastic according to the prior results from the FE cube simulation with the following adjustments: Only five data points from Fig. 11 in the range $-0.022 < \epsilon < -0.007$ are used (enclosed by the black dashed rectangle in Fig. 11). This data is chosen, because it governs the strongly nonlinear-elastic behavior. The stresses σ_X and strains ϵ_X within it are scaled with factor 0.2 to ensure that the nonlinear behavior is fully activated during the simulation. The corresponding scaled stress–strain data (five points) are plotted in Fig. 12b. A sixth data point is added manually in the origin (0,0), so that the initial stiffness complies exactly with the Young's modulus $E = 73000$ N/mm^2 for reasons of comparison. By doing so, the authors make sure that when the LF excitation X_Ω approaches zero in the simulation, nonlinearity (3) the contact of fatigue crack surfaces does not affect the dynamic properties of the system.

In the next step, a simulation is run where the two red volumes in Fig. 12a behave according to the stress–strain data in Fig. 12b while the rest of the specimen behaves linearly-elastic with $E = 73000$ N/mm^2. All other settings comply with the previous simulations in Sections 4.2 and 4.3 corresponding to nonlinearities (1) and (2). The results are plotted in Fig. 13. The stress σ_X in closest vicinity of the sensing node is plotted in Fig. 13a and represents the LF excitation X_Ω. Fig. 13b shows the coordinate system with the specimen in the FE model for orientation. In Fig. 13c the results from the first simulation only governing (1) the variation of geometric stiffness are presented with the corresponding FFT spectrum in dB in Fig. 13d. The results from the third simulation — governing the variation of geometric stiffness and the contact of fatigue crack surfaces — are shown analogously in Fig. 13e (system

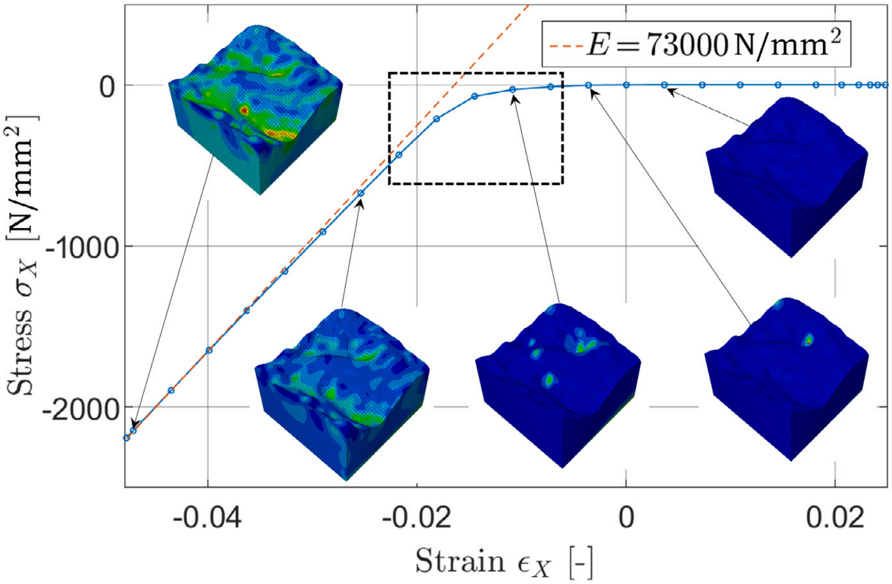

Fig. 11. Stress vs. strain results (blue solid line) for the cube parts pressed against each other in X-direction (with the lateral offset); Linear reference (red dashed line) corresponding to the stiffness $E = 73000$ N/mm^2; The black dashed rectangle indicates the five data points that are used in the following step. (For interpretation of the references to color in this figure legend, the reader is referred to the web version of this article.)

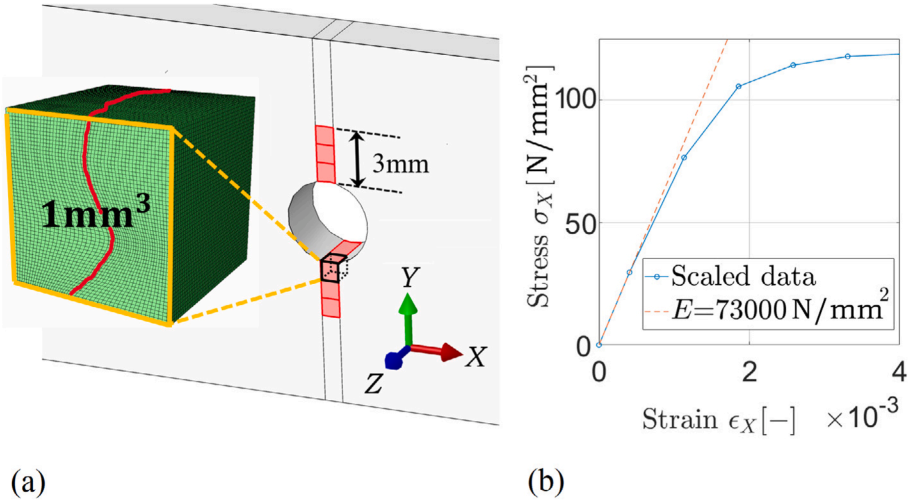

Fig. 12. (a) Detail of the FE model around the notch: The highlighted red volumes represent volumes that are separated by a fatigue crack (b) Scaled stress–strain data (scaling factor 0.2) from the previous cube simulation. The data point in the origin (0,0) was added manually for reasons of comparison. (For interpretation of the references to color in this figure legend, the reader is referred to the web version of this article.)

response in time domain) and Fig. 13f (FFT spectrum). When σ_X in Fig. 13a approaches zero, the nonlinearities do not affect the system properties. Therefore, the amplitudes in the corresponding system responses are identical for a moment.

It can be seen in time domain that the nonlinear behavior of such a small volume affects the global system response significantly in terms of modulation. Note that also in this case the amplitude modulation (AM) caused by the variation of geometric stiffness and the contact of fatigue crack surfaces work in opposite directions, as expected on the basis of the suggested analytical explanation. In fact, this result demonstrates that the modulation caused by the contact of fatigue crack surfaces is significantly stronger than the modulation caused by the variation of geometric stiffness. If the nonlinearities were equally strong, the modulations would neutralize each other. Conventional quantification of the spectrum with $MI = -21.6$ dB would not allow detection of the fatigue crack, because the increase $\Delta MI = 0.6$ dB is negligibly small. This demonstrates that the conventional evaluation technique is error prone.

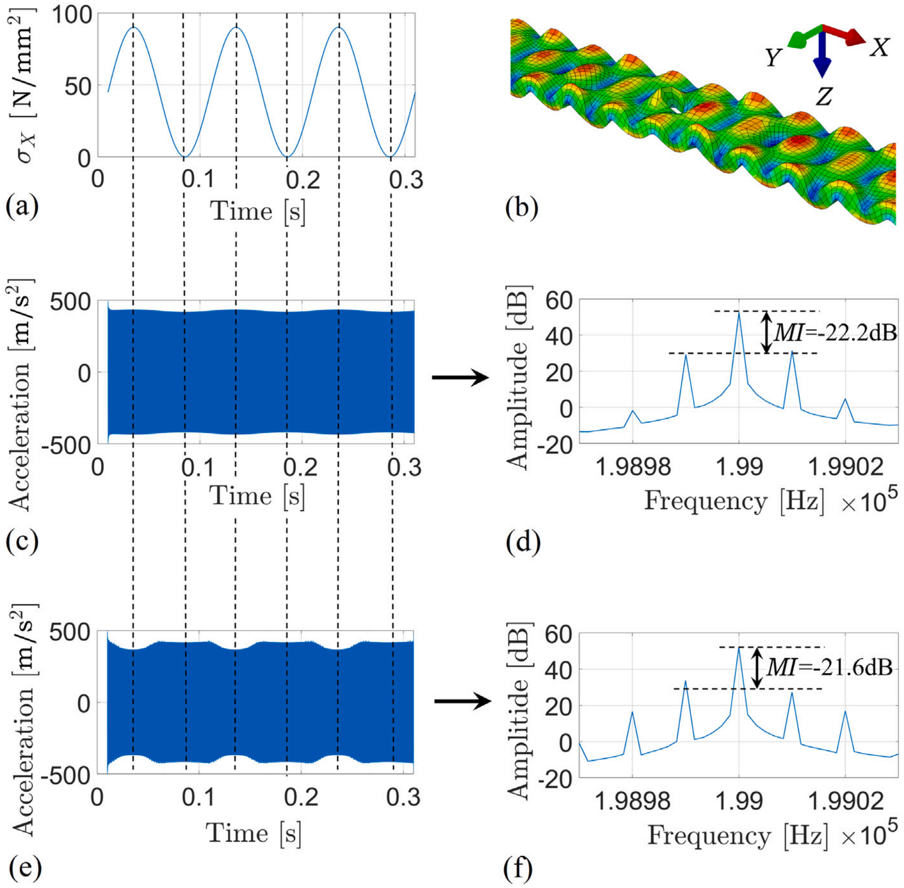

Fig. 13. (a) Stress σ_X over time in direct vicinity of the sensing node (b) Coordinate system for orientation; deformation of the specimen is magnified by factor $2.5 \cdot 10^7$ (c) System response (acceleration in Z-direction) at the sensing node (the only present nonlinearity in this simulation is the variation of geometric stiffness) (d) Corresponding FFT spectrum in dB (e) System response (acceleration in Z-direction) at the sensing node (the present nonlinearities in this simulation are the variation of geometric stiffness and the contact of fatigue crack surfaces) (f) Corresponding FFT spectrum in dB.

4.5. Combination of all three nonlinearities

Finally, a simulation is run with all three nonlinearities combined in the same system. The results are plotted in Figs. 14e and 14f. Figs. 14c and 14d show the results from the simulation only governing the first two nonlinearities. Comparison of the results in time domain (Figs. 14c vs. 14e) reveals that the "additional" nonlinearity introduced by the fatigue crack increases the AM in the system response. The MI evaluated from the corresponding FFT spectra, however, do not display such an increase in terms of modulation. In fact, evaluation of the spectrum in 14d (without crack) leads to the value $MI = +11.0$ dB while the spectrum in Fig. 14f (with crack) only leads to the value $MI = +8.1$ dB. Note that the spectra from both simulations show over one hundred pairs of sidebands governing the modulation. The MI however only takes into account the first pair at $\omega \pm \Omega$. This demonstrates that an additional nonlinearity in the system (here: the crack) does not necessarily increase the MI. It emphasizes the prior conclusion that the conventional monitoring approach is error prone.

5. Conclusions and outlook

It was explained analytically why two nonlinearities working in opposite directions (one stiffening the structure under loading, one softening it) cause contrary modulations: The two nonlinear contributions can neutralize each other in the system response. It has to be concluded that the presence of two nonlinearities in the same system does not necessarily cause more modulation in the system response than both nonlinearities would individually. Afterwards, the relevance and occurrence of contrary modulations was demonstrated numerically for an aluminum plate. Three nonlinearities that are present in the plate were investigated separately: (1) The variation of geometric stiffness, (2) the nonlinear-elastic behavior of aluminum and (3) the contact of fatigue crack surfaces. While nonlinearity (1) is stiffening the structure with tensile loading, nonlinearities (2) and (3) are softening it. The modulation caused by them individually was quantified and compared. In case of the second nonlinearity — the nonlinear-elastic material behavior of aluminum — experimental test data was taken into account to model it accurately. For the third nonlinearity — the

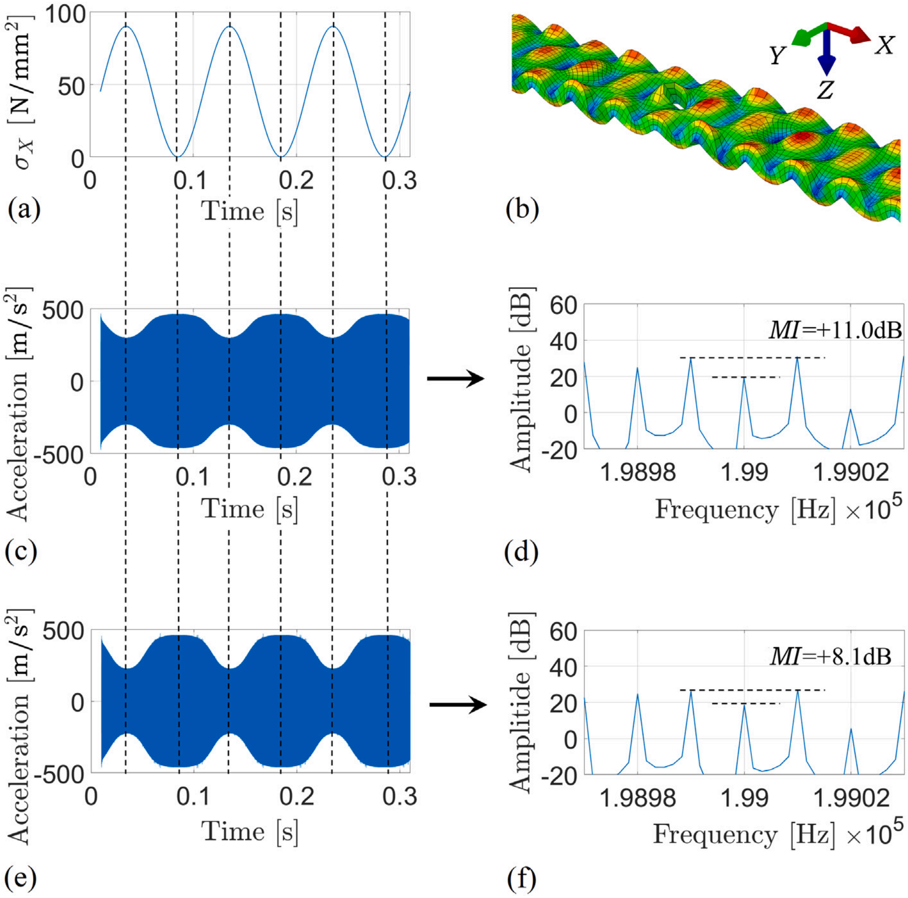

Fig. 14. (a) Stress σ_X over time in direct vicinity of the sensing node (b) Coordinate system for orientation; deformation of the specimen is magnified by factor $2.5 \cdot 10^7$ (c) System response (acceleration in Z-direction) at the sensing node (the present nonlinearities in this simulation are the variation of geometric stiffness and the nonlinear-elastic behavior of aluminum) (d) Corresponding FFT spectrum in dB (e) System response (acceleration in Z-direction) at the sensing node (the present nonlinearities in this simulation are the variation of geometric stiffness and the nonlinear-elastic material behavior of aluminum and the contact of fatigue crack surfaces) (f) Corresponding FFT spectrum in dB.

contact of fatigue crack surfaces — experimental microscope data was presented that describes the three-dimensional geometry of a fatigue crack surface in aluminum. The geometry was used to explain and demonstrate numerically why and how nonlinear such contact may behave under (external) tensile fatigue loading. The results were utilized to define the nonlinear-elastic material of a local volume in the model representing the crack. The comparison of the numerical results demonstrates that the modulation caused by nonlinearity (1) is, as expected, contrary to the modulations caused by the nonlinearities (2) and (3). Consequently, the superposition of the modulations does not lead to the result that is expected by most state-of-the-art VAM applications. This finding complies with the analytical explanation and indicates that the conventional monitoring approach of monitoring an increase of sideband amplitudes over the lifetime of a structure is error prone. It must be concluded that damage-induced modulation does not necessarily increase the total modulation in the system response. Future work should exploit the evaluation of the system response in time domain while taking into account the occurrence of contrary modulations. The presented findings can serve as a basis.

CRediT authorship contribution statement

Lennart Dorendorf: Writing – review & editing, Writing – original draft, Investigation, Conceptualization. **Nikolay Lalkovski:** Writing – review & editing, Validation, Supervision, Methodology, Conceptualization. **Benjamin Boll:** Writing – review & editing, Investigation, Data curation, Conceptualization. **Marcus Rutner:** Writing – review & editing, Validation, Supervision, Funding acquisition.

Declaration of competing interest

The authors declare that they have no known competing financial interests or personal relationships that could have appeared to influence the work reported in this paper.

Acknowledgments

The authors thank the Deutsche Forschungsgemeinschaft (DFG), Germany for financial support of this research (project number: 457416916).

Data availability

Data will be made available on request.

References

[1] O. Rudenko, A. Chin, Nonlinear acoustic properties of a rough surface contact and acoustiodiagnostics of a roughness height distribution, Acoust. Phys. 1994 (1994).

[2] V.Y. Zaitsev, A.M. Sutin, I.Y. Belyaeva, V.E. Nazarov, Nonlinear interaction of acoustical waves due to cracks and its possible usage for cracks detection, Modal Anal. 1 (3) (1995) 335–344, http://dx.doi.org/10.1177/107754639500100305.

[3] V.E. Nazarov, A.M. Sutin, Nonlinear elastic constants of solids with cracks, J. Acoust. Soc. Am. 102 (6) (1997) 3349–3354, http://dx.doi.org/10.1121/1.419577.

[4] D.M. Donskoy, A.M. Sutin, Vibro-acoustic modulation nondestructive evaluation technique, J. Intell. Mater. Syst. Struct. 9 (9) (1998) 765–771, http://dx.doi.org/10.1177/1045389X9800900909.

[5] A.E. Ekimov, I.N. Didenkulov, V. v. Kazakov, Modulation of torsional waves in a rod with a crack, J. Acoust. Soc. Am. 106 (3) (1999) 1289–1292, http://dx.doi.org/10.1121/1.427163.

[6] L. Pieczonka, A. Klepka, A. Martowicz, W.J. Staszewski, Nonlinear vibroacoustic wave modulations for structural damage detection: an overview, Opt. Eng., Bellingham 55 (1) (2016) 011005, http://dx.doi.org/10.1117/1.OE.55.1.011005.

[7] D.M. Donskoy, A.M. Sutin, A.E. Ekimov, Nonlinear acoustic interaction on contact interfaces and its use for nondestructive testing, NDT E Int. 34 (4) (2001) 231–238, http://dx.doi.org/10.1016/S0963-8695(00)00063-3.

[8] A. Klepka, W.J. Staszewski, R.B. Jenal, M. Szwedo, J. Iwaniec, T. Uhl, Nonlinear acoustics for fatigue crack detection – experimental investigations of vibro-acoustic wave modulations, Struct. Heal. Monit.: Int. J. 11 (2) (2012) 197–211, http://dx.doi.org/10.1177/1475921711414236.

[9] H.J. Lim, H. Sohn, Necessary conditions for nonlinear ultrasonic modulation generation given a localized fatigue crack in a plate-like structure, Mater. (Basel, Switzerland) 10 (3) (2017) http://dx.doi.org/10.3390/ma10030248.

[10] K. Dziedziech, A. Klepka, J. Roemer, L. Pieczonka, Experimental study of thermo-acoustic wave modulation in a cracked plate, J. Sound Vib. 498 (2021) 115970, http://dx.doi.org/10.1016/j.jsv.2021.115970.

[11] M. Meo, U. Polimeno, G. Zumpano, Detecting damage in composite material using nonlinear elastic wave spectroscopy methods, Appl. Compos. Mater. 15 (3) (2008) 115–126, http://dx.doi.org/10.1007/s10443-008-9061-7.

[12] F. Aymerich, W.J. Staszewski, Experimental study of impact-damage detection in composite laminates using a cross-modulation vibro-acoustic technique, Struct. Heal. Monit.: Int. J. 9 (6) (2010) 541–553, http://dx.doi.org/10.1177/1475921710365433.

[13] Y. He, Y. Xiao, Z. Su, Y. Pan, Z. Zhang, Contact acoustic nonlinearity effect on the vibro-acoustic modulation of delaminated composite structures, Mech. Syst. Signal Process. 163 (2022) 108161, http://dx.doi.org/10.1016/j.ymssp.2021.108161.

[14] S. Kim, D.E. Adams, H. Sohn, G. Rodriguez-Rivera, N. Myrent, R. Bond, J. Vitek, S. Carr, A. Grama, J.J. Meyer, Crack detection technique for operating wind turbine blades using Vibro-Acoustic Modulation, Struct. Heal. Monit.: Int. J. 13 (6) (2014) 660–670, http://dx.doi.org/10.1177/1475921714553732.

[15] T. Ooijevaar, M.D. Rogge, R. Loendersloot, L. Warnet, R. Akkerman, T. Tinga, Vibro-acoustic modulation–based damage identification in a composite skin–stiffener structure, Struct. Heal. Monit.: Int. J. 15 (4) (2016) 458–472, http://dx.doi.org/10.1177/1475921716645107.

[16] L. Wei, J. Chen, Determination of optimal probing frequency for enhancing nonlinear vibro-acoustic modulation behaviors of delaminated CFRP based on local defect resonance, Mech. Syst. Signal Process. 187 (2023) 109961, http://dx.doi.org/10.1016/j.ymssp.2022.109961.

[17] A. Klepka, L. Pieczonka, W.J. Staszewski, F. Aymerich, Impact damage detection in laminated composites by non-linear vibro-acoustic wave modulations, Compos. Part B: Eng. 65 (2014) 99–108, http://dx.doi.org/10.1016/j.compositesb.2013.11.003.

[18] B. Boll, E. Willmann, B. Fiedler, R.H. Meißner, Weak adhesion detection – Enhancing the analysis of vibroacoustic modulation by machine learning, Compos. Struct. 273 (2021) 114233, http://dx.doi.org/10.1016/j.compstruct.2021.114233.

[19] P. Duffour, M. Morbidini, P. Cawley, A study of the vibro-acoustic modulation technique for the detection of cracks in metals, J. Acoust. Soc. Am. 119 (3) (2006) 1463, http://dx.doi.org/10.1121/1.2161429, URL https://asa.scitation.org/doi/pdf/10.1121/1.2161429.

[20] U. Polimeno, M. Meo, Understanding the effect of boundary conditions on damage identification process when using non-linear elastic wave spectroscopy methods, Int. J. Non-Linear Mech. 43 (3) (2008) 187–193, http://dx.doi.org/10.1016/j.ijnonlinmec.2007.12.013.

[21] V.Y. Zaitsev, L.A. Matveev, A.L. Matveyev, On the ultimate sensitivity of nonlinear-modulation method of crack detection, NDT E Int. 42 (7) (2009) 622–629, http://dx.doi.org/10.1016/j.ndteint.2009.05.001.

[22] N.C. Yoder, D.E. Adams, Vibro-acoustic modulation utilizing a swept probing signal for robust crack detection, Struct. Heal. Monit.: Int. J. 9 (3) (2010) 257–267, http://dx.doi.org/10.1177/1475921710365261.

[23] M. Dunn, A. Carcione, P. Blanloeuil, M. Veidt, Critical aspects of experimental damage detection methodologies using nonlinear vibro-ultrasonics, Procedia Eng. 188 (2017) 133–140, http://dx.doi.org/10.1016/j.proeng.2017.04.466.

[24] L. Dorendorf, N. Lalkovski, M. Rutner, Physical explanation for vibro-acoustic modulation due to local and global nonlinearities in a structure and its experimental and numerical validation, J. Sound Vib. 528 (2022) 116885, http://dx.doi.org/10.1016/j.jsv.2022.116885.

[25] V.Y. Zaitsev, P. Sas, Nonlinear response of a weakly damaged metal sample: A dissipative modulation mechanism of vibro-acoustic interaction, J. Vib. Control 6 (6) (2000) 803–822, http://dx.doi.org/10.1177/107754630000600601.

[26] D.M. Donskoy, Nonlinear acoustic methods, in: C. Boller, F.-K. Chang, Y. Fujino (Eds.), in: Encyclopedia of Structural Health Monitoring, vol. 1, John Wiley & Sons, Ltd, Chichester, UK, 2009.

[27] B. Boll, L. Dorendorf, P. Oppermann, E. Willmann, B. Fieder, B.-C. Renner, M. Rutner, R.H. Meißner, Synthetic generation of vibroacoustic modulation signals for structural health monitoring applications, Mech. Syst. Signal Process. 200 (2023) http://dx.doi.org/10.1016/j.ymssp.2023.110498.

[28] R.W. Clough, J. Penzien, Dynamics of Structures, second ed., McGraw-Hill, New York, 2004, reprint.

[29] Z. Jastrzebski, The Nature and Properties of Engineering Materials, Wiley, 1987.

[30] G.I. for Standardization, DIN 50125:2016-12, Testing of metallic materials – Tensile test pieces.

[31] SIMULIA, Abaqus 6.14 Documentation - Abaqus Analysis User's Guide, Dassault Systemes, Vélizy-Villacoublay, France, 2014.

[32] J.-Y. Kim, V.A. Yakovlev, S.I. Rokhlin, Parametric modulation mechanism of surface acoustic wave on a partially closed crack, Appl. Phys. Lett. 82 (19) (2003) 3203, http://dx.doi.org/10.1063/1.1572552, URL https://aip.scitation.org/doi/pdf/10.1063/1.1572552.